Mechanisms and Machine Science

Pierre Larochelle
J. Michael McCarthy
Craig P. Lusk *Editors*

Proceedings of MSR-RoManSy 2024

Combined IFToMM Symposium of RoManSy and USCToMM Symposium on Mechanical Systems and Robotics

IFToMM

Springer

Mechanisms and Machine Science

Volume 159

This book series establishes a well-defined forum for monographs, edited Books, and proceedings on mechanical engineering with particular emphasis on MMS (Mechanism and Machine Science). The final goal is the publication of research that shows the development of mechanical engineering and particularly MMS in all technical aspects, even in very recent assessments. Published works share an approach by which technical details and formulation are discussed, and discuss modern formalisms with the aim to circulate research and technical achievements for use in professional, research, academic, and teaching activities.

This technical approach is an essential characteristic of the series. By discussing technical details and formulations in terms of modern formalisms, the possibility is created not only to show technical developments but also to explain achievements for technical teaching and research activity today and for the future.

The book series is intended to collect technical views on developments of the broad field of MMS in a unique frame that can be seen in its totality as an Encyclopaedia of MMS but with the additional purpose of archiving and teaching MMS achievements. Therefore, the book series will be of use not only for researchers and teachers in Mechanical Engineering but also for professionals and students for their formation and future work.

The series is promoted under the auspices of International Federation for the Promotion of Mechanism and Machine Science (IFToMM).

Prospective authors and editors can contact Mr. Pierpaolo Riva (publishing editor, Springer) at: pierpaolo.riva@springer.com

Indexed by SCOPUS and Google Scholar.

Pierre Larochelle · J. Michael McCarthy ·
Craig P. Lusk
Editors

Proceedings of MSR-RoManSy 2024

Combined IFToMM Symposium of RoManSy and USCToMM Symposium on Mechanical Systems and Robotics

Springer

Editors
Pierre Larochelle
Department of Mechanical Engineering
South Dakota School of Mines
and Technology
Rapid City, SD, USA

J. Michael McCarthy
University of California
Irvine, CA, USA

Craig P. Lusk
Department of Mechanical Engineering
University of South Florida
Tampa, FL, USA

ISSN 2211-0984 ISSN 2211-0992 (electronic)
Mechanisms and Machine Science
ISBN 978-3-031-60617-5 ISBN 978-3-031-60618-2 (eBook)
https://doi.org/10.1007/978-3-031-60618-2

This Springer imprint is published by the registered company Springer Nature Switzerland AG
The registered company address is: Gewerbestrasse 11, 6330 Cham, Switzerland

Preface

This volume constitutes the refereed conference proceedings of the Joint Mechanical Systems and Robotics and RoManSy Symposium, MSR-RoManSy 2024, held in Saint Petersburg, Florida, United States, in May 2024. In 2024, there was an exciting synergistic combining of MSR and RoManSy. RoManSy is a long-established series of conferences traditionally held in Europe. This 2024 conference, combining both MSR and RoManSy, is the 25th RoManSy gathering and the 3rd MSR gathering.

The joint MSR-RoManSy Symposium welcomed submissions that addressed: Specialized Robotic Systems; Soft, Wearable & Origami Robotic Systems; Applications to Walking, Flying, Climbing, Ground, Underground, Swimming, & Space Systems; Human Rehabilitation & Performance Augmentation; Design and Analysis of Mechanisms & Machines; Human-Robot Collaborative Systems; Service Robotics; Mechanical Systems & Robotics Education; Commercialization of Mechanical Systems & Robotics; and related topics.

MSR-RoManSy 2024 was organized under the patronage of the U.S. Committee for the Theory of Machines and Mechanisms (USCToMM), the Canadian Committee for the Theory of Machines and Mechanisms (CCToMM), and the IFToMM Technical Committee on Robotics and Mechatronics. The goal of USCToMM is to promote research and development in the field of machines and mechanisms by theoretical and experimental methods, along with their practical application. USCToMM is the United States' Member Organization of the International Federation for the Promotion of Mechanism and Machine Science (IFToMM).

Every other year, USCToMM organizes a MSR symposium to bring together researchers from the US, Canada, Mexico, and from around the globe to share their latest research results, exchange new ideas, and foster new collaborations. The USCToMM symposia bring together researchers in all areas of mechanisms, machines, mechanical systems, and robotics for an engaging and focused academic experience. In this publication, the editors introduce 19 full papers that were carefully reviewed, presented, and deeply discussed during single-track sessions at MSR-RoManSy 2024.

We wish to express our sincere thanks to the authors, reviewers, and participants for making the combined 3rd USCToMM MSR and 25th RoManSy Symposium a success.

Rapid City, USA	Pierre Larochelle
Irvine, USA	J. Michael McCarthy
Tampa, USA	Craig P. Lusk

Contents

Chapter 1
Kinematic Analysis of a Novel Actuation Redundant 3-DOF Parallel Manipulator Based on Parallelogram-Linkage

Qi Zou, Shuo Zhang, Yuancheng Shi, and Byung-Ju Yi

Abstract The passive joints occurring in the parallel robots require additional steps to be calculated, which may lead to complicated analytical kinematic and dynamic models, become burdens to derive these mathematical solutions or demand extra efforts to measure their motions. This research presents a special planar parallel manipulator with actuation redundancy based on parallelogram linkage. Every moving linkage excluding the mobile platform is parallel to one of the actuation rods within the reachable workspace and all these passive joint angles can be conveniently resolved from the active joint angles through simple arithmetic operations. The constant linkage dimension relationships are utilized to formulate the inverse kinematic solution with the assistance of two additional virtual points. The vector loop equations are employed to compute the forward kinematic results. The Jacobian matrix is established from the forward kinematic model. The spatial searching methodology is utilized to obtain the reachable workspace and the kinematic performance distributions are explored.

Keywords Parallel manipulator · Parallelogram linkage · Redundant robot · Performance evaluation

1.1 Introduction

A conventional parallel robot is constituted of a fixed platform and moving platform connected by several kinematic chains. Each kinematic limb is generally actuated by only one motor, which is different from the serial robot where each joint

Q. Zou
Robotics Engineering, Columbus State University, Columbus, GA 31907, USA

S. Zhang
Lassonde School of Engineering, York University, Toronto, ON M3J 1P3, Canada

Y. Shi · B.-J. Yi (✉)
School of Electrical Engineering, Hanyang University, Ansan 15588, Korea
e-mail: bj@hanyang.ac.kr

P. Larochelle et al. (eds.), *Proceedings of MSR-RoManSy 2024*, Mechanisms and Machine Science 159, https://doi.org/10.1007/978-3-031-60618-2_1

demands a motor. Compared with the serial robot in the similar scale and materials, the parallel robot tends to realize higher stiffness, payload performance, precision level and speed/acceleration [1, 2]. The parallel robots are widely employed in parallel kinematic machine tools [3], stacking robots [4] and medical robots [5].

The most distinguished drawbacks of parallel robots contain the restricted reachable workspace and complex mathematical solution. The methodologies to overcome the limited workspace include designing novel robot architectures, utilizing the equivalent joints to replace the spatial joints (i.e., use two orthogonal revolute joints to substitute a universal joint). The latter issue happens especially on the forward kinematic models due to a group of nonlinear equations. There are some strategies, analytical methods (e.g., Sylvester's dialytic elimination algorithm [6]), numerical methods (e.g., Newton–Raphson method) [7], Newton-Gauss method [8]), artificial intelligent algorithms (e.g., support vector machine approach [9]).

The difficulty of the nonlinear analytical forward kinematic problem can be fully/partially alleviated if there are some special relationships among some moving linkages. Under this condition, some passive joint angles can be conveniently formulated, which may be beneficial to derive the first- or second- order kinematic problems with sufficient computation efficiency.

The noncomplex forward kinematic solutions can be guaranteed in some parallel architectures where special modules are employed in the kinematic chains. For example, the parallelogram mechanism has been widely utilized many parallel and serial robots, such as the Diamond robot [10], rotary Delta robot [11], Linear Delta robot [12], Improved variants of Delta robot (Par4, H4, I4 family [13]), University of Maryland robot [14], the parallel manipulator with Schönflies motion [15], 2 degrees-of-freedom (DOFs) parallel structure [16].

The additional internal constraints (parallel relationship between two opposite rods) originated from the parallelogram linkages can facilitate the calculation of forward kinematic models. Another function of the parallelogram linkage is to enhance the stiffness of the kinematic chain. As a special case, the Rhombus linkage is another special module which is popular in parallel robots, especially in deployable mechanisms (e.g., the Expteron robot [17], D-SLiM [18]) where large workspace and small storage space are desired.

The parallel manipulator with actuation redundancy has received increasing interests recently. It is reported that this feature could enhance the stiffness of the whole structure, supply better force capacity and avoid some singularities with active manner, at the expense of complicated control strategy for actuation joints forces/torques [19, 20].

This paper aims to mitigate the unknown passive joints calculation and complex forward kinematics by special design using parallelogram linkages. Each moving linkage excluding the moving platform is parallel to one of the driving linkages when the mobile platform is in any pose. The layout of this manuscript is organized as follows. The detailed kinematic models are derived in Sect. 1.2, followed by the workspace and kinematic analysis in Sects. 1.3 and 1.4, respectively. This work is concluded in Sect. 1.5.

1.2 Position Analysis

1.2.1 Inverse Kinematics

The proposed planar parallel structure with two kinematic limbs is seen in Fig. 1.1a. Each kinematic limb is constituted of six linkages (A_iC_i, C_iI_i, D_iE_i, E_iF_i, B_iH_i, and H_iP_i, i = 1,2) and nine revolute joints (locating at points A_i, B_i, C_i, D_i, E_i, F_i, H_i, I_i and P_i, i = 1,2). In each kineamtic limb, the proximal end of linakge A_iC_i is attached to the fixed platform A_1A_2, while the distal end is connected to the linkage C_iI_i. Point I_i is on the linkage H_iP_i, which is connected to the mobile platform P_1P_2 by a revolute joint. Linakges A_iC_i and H_iP_i can also be connected by a middle inkage B_iH_i. The fixed platform can also reach to the link C_iI_i through linkage D_iE_i and then linkage E_iF_i. The key construction principles of each kinematic limb within this symmetrical parallel mechanism are listed below (i = 1 or 2),

(a) There are two parallelogram linkages in each kinematic chain. They are composed of the points B_i-C_i-I_i-H_i and D_i-E_i-F_i-C_i, respectively. Linkages A_iC_i, E_iF_i, and H_iP_i are paraellel. Linkage A_iE_i, B_iH_i, and C_iI_i are collinear.
(b) Points B_i and D_i lie at line A_iC_i.
(e) Point F_i is on the line C_iI_i.
(f) Point P_i is collinear with line H_iI_i.

The linkage lengths are listed as: $|A_iB_i| = L_1$, $|B_iC_i| = |H_iI_i| = L_2$, $|C_iF_i| = L_3$, $|F_iI_i| = L_4$, $|I_iP_i| = L_7$, $|P_iP| = L_8$ (i = 1,2). The global coordiate system is constructed, as illustratd in Fig. 1.1a. The X-axis is collinear with the fixed platform A_1A_2, while the Y-axis is vertical. The coordinate of point D_1 is (L_5,L_6). In this case, point D_1 coincides with point A_1 in the first kineamtic chain and point D_2 coincides with point A_2 in the second kineatmic chain. Therefore, $L_5 = L_6 = 0$. The coordinates of the points A_1 and A_2 are separately (x_{A1},0) and (x_{A2},0). The system input of this parallel manipulator is denoted as the rotation angles $\mathbf{Q} = [\theta_1; \theta_2; \theta_3; \theta_4]$ at four points, A_1, D_1, A_2 and D_2, with respect to the X axis. The position and orientation of the mobile platform P_1PP_2 are summaried as $\mathbf{X} = [x; y; \alpha]$ in the planar coordinate system. This parallel architecture is classified as the actuation redundant robot since there is one additional motor to manipulate the mobile platform.

Given the pose $\boldsymbol{X}$ of the mobile platform, the inverse kineamtic model is to derive the four rotation angles of linakges A_1C_1, D_1E_1, A_2C_1 and D_2E_2. For the sake of simplicity, two virtual points G_1 and G_2 are attached to this planar parallel mechanism, as illustrated in Fig. 1.1a. Two revolute joints are mounted at points G_1 and G_2, respectively. The virtual links C_iG_i and G_iP_i (i = 1,2) are separately defined as L_7 and $L_3 + L_4$. Thus, a new parallelogram mechanims is established by points $C_iI_iP_iG_i$ in each kineamtic limb. In accordance with the parallelgoram mechanisms employed in this design, linkage C_iG_i is parallel to linkages A_iC_i, E_iF_i and H_iP_i, while linkage G_iP_i is collinear with linkages D_iE_i, B_iH_i and C_iI_i in each kinematic chain. These two added points can enable the decoupled calculations of two unknown joint angles in each kinematic chain and simplify the inverse kinematic solution.

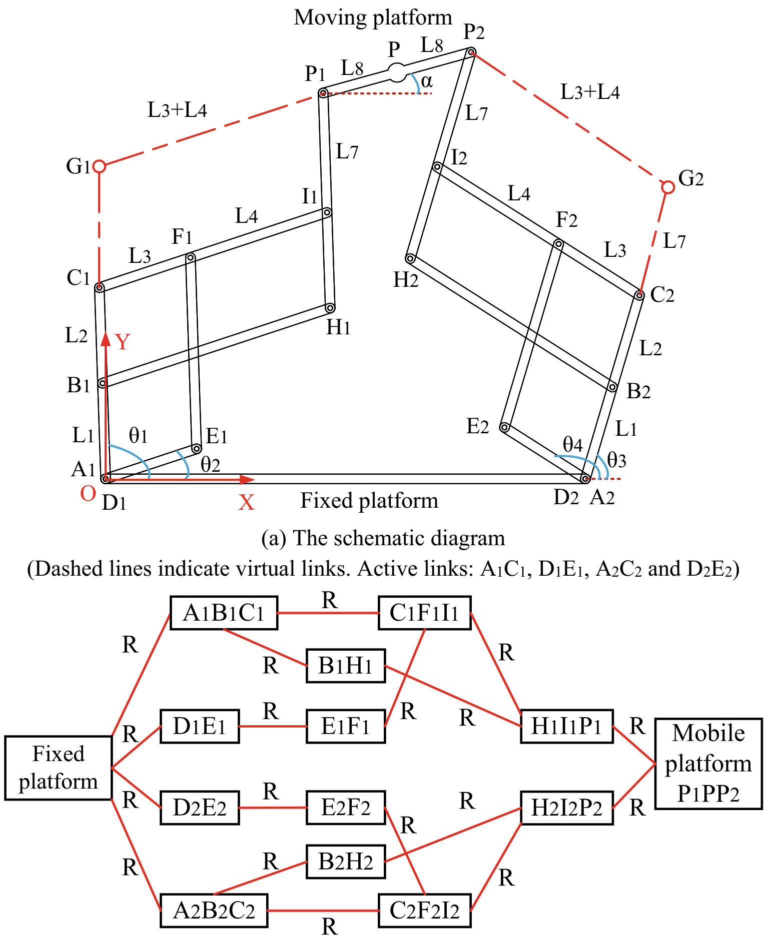

(a) The schematic diagram
(Dashed lines indicate virtual links. Active links: A_1C_1, D_1E_1, A_2C_2 and D_2E_2)

(b) The topology graph (R denotes Rotary joint)

Fig. 1.1 The planar parallel robot

To compute θ_1 in the first kineamtic limb, the following constraint equation can be generated

$$\|\mathbf{OP}_1 - \mathbf{OG}_1\| = \|\mathbf{G}_1\mathbf{P}_1\| = L_3 + L_4 \tag{1.1}$$

where the $\|\ \|$ symbol denotes 2-norm operation.

Two vector-loop equations should be explored to determine the two vectors in the left side of Eq. (1.1). In according to the geometry of this parallel robot, the position of point G_1 is calculated

$$\mathbf{OG}_1 = \mathbf{OA}_1 + \mathbf{A}_1\mathbf{G}_1 = \begin{pmatrix} x_{A1} + (L_1 + L_2 + L_7)\cos\theta_1 \\ (L_1 + L_2 + L_7)\sin\theta_1 \end{pmatrix} \tag{1.2}$$

The position of point P_1 is derived as

$$\mathbf{OP}_1 = \mathbf{OP} + \mathbf{P}_1\mathbf{P} = \begin{pmatrix} x - L_8\cos\alpha \\ y - L_8\sin\alpha \end{pmatrix} \tag{1.3}$$

Combing Eqs. (1.1–1.3), the following equation can be generated

$$N_{11}\sin\theta_1 + N_{12}\cos\theta_1 + N_{13} = 0 \tag{1.4}$$

where

$$\begin{cases} N_{11} = -2(y - L_8\sin\alpha)(L_1 + L_2 + L_7) \\ N_{12} = -2(x - x_{A1} - L_8\cos\alpha)(L_1 + L_2 + L_7) \\ N_{13} = (x - L_8\cos\alpha - x_{A1})^2 + (y - L_8\sin\alpha)^2 + (L_1 + L_2 + L_7)^2 - (L_3 + L_4)^2 \end{cases}$$

A special substitution should be utilized to solve Eq. (1.4),

$$t_1 = \tan(\theta_1/2) \tag{1.5}$$

On the basis of trigonometric identity, the following equations can be expressed,

$$\sin\theta_1 = 2t_1/(1 + t_1^2),\ \cos\theta_1 = (1 - t_1^2)/(1 + t_1^2) \tag{1.6}$$

Combing Eqs. (1.4) and (1.6) yields the following quadratic equation of variable t_1,

$$(N_{13} - N_{12})t_1^2 + 2N_{11}t_1 + (N_{12} + N_{13}) = 0 \tag{1.7}$$

The variable t_1 can be formulated directly from Eq. (1.7),

$$t_1 = \frac{-N_{11} \pm \sqrt{N_{11}^2 + N_{12}^2 - N_{13}^2}}{N_{13} - N_{12}} \tag{1.8}$$

The actuation angle θ_1 is then deduced based on Eq. (1.5),

$$\theta_1 = 2\tan^{-1} t_1 \tag{1.9}$$

The second constraint equation to solve rotatioanl angle θ_2 is arranged as

$$\|\mathbf{OG}_1 - \mathbf{OA}_1\| = \|\mathbf{A}_1\mathbf{G}_1\| = L_1 + L_2 + L_7 \tag{1.10}$$

The vector $\mathbf{OG}_1$ should be different from the expression in Eq. (1.2), in order to express explicitly the rotation angle θ_2, as seen below

$$\mathbf{OG}_1 = \mathbf{OP}_1 - \mathbf{G}_1\mathbf{P}_1 = \begin{pmatrix} x - L_8 \cos\alpha - (L_3 + L_4)\cos\theta_2 \\ y - L_8 \sin\alpha - (L_3 + L_4)\sin\theta_2 \end{pmatrix} \tag{1.11}$$

Akin to the calculation process in Eqs. (1.4–1.9) for the angle θ_1, the rotation angle θ_2 can be resolved as

$$\theta_2 = 2\tan^{-1}\frac{-N_{21} \pm \sqrt{N_{21}^2 + N_{22}^2 - N_{23}^2}}{N_{23} - N_{22}} \tag{1.12}$$

where

$$\begin{cases} N_{21} = -2(y - L_8 \sin\alpha)(L_3 + L_4) \\ N_{22} = -2(x - x_{A1} - L_8 \cos\alpha)(L_3 + L_4) \\ N_{23} = (x - L_8 \cos\alpha - x_{A1})^2 + (y - L_8 \sin\alpha)^2 + (L_3 + L_4)^2 - (L_1 + L_2 + L_7)^2 \end{cases}$$

In a simialr manner, the first constraint equation of the second kinematic limb is established as

$$\|\mathbf{OP}_2 - \mathbf{OG}_2\| = \|\mathbf{G}_2\mathbf{P}_2\| = L_3 + L_4 \tag{1.13}$$

where

$$\begin{cases} \mathbf{OP}_2 = \mathbf{OP} + \mathbf{PP}_2 = \begin{pmatrix} x + L_8 \cos\alpha \\ y + L_8 \sin\alpha \end{pmatrix} \\ \mathbf{OG}_2 = \mathbf{OA}_2 + \mathbf{A}_2\mathbf{G}_2 = \begin{pmatrix} x_{A2} + (L_1 + L_2 + L_7)\cos\theta_3 \\ (L_1 + L_2 + L_7)\sin\theta_3 \end{pmatrix} \end{cases}$$

Arranging Eq. (1.13) in a similar form as Eq. (1.4), the rotation angle θ_3 is formulated as

$$\theta_3 = 2\tan^{-1}\frac{-N_{31} \pm \sqrt{N_{31}^2 + N_{32}^2 - N_{33}^2}}{N_{33} - N_{32}} \tag{1.14}$$

where

$$\begin{cases} N_{31} = -2(y + L_8 \sin\alpha)(L_1 + L_2 + L_7) \\ N_{32} = -2(x + L_8 \cos\alpha - x_{A2})(L_1 + L_2 + L_7) \\ N_{33} = (x + L_8 \cos\alpha - x_{A2})^2 + (y + L_8 \sin\alpha)^2 + (L_1 + L_2 + L_7)^2 - (L_3 + L_4)^2 \end{cases}$$

Another constraint equation of the second kinematic chain is described as

$$\|\mathbf{OG}_2 - \mathbf{OA}_2\| = \|\mathbf{A}_2\mathbf{G}_2\| = L_1 + L_2 + L_7 \tag{1.15}$$

where

$$\mathbf{OG}_2 = \mathbf{OP}_2 - \mathbf{G}_2\mathbf{P}_2 = \begin{pmatrix} x + L_8 \cos\alpha - (L_3 + L_4)\cos\theta_4 \\ y + L_8 \sin\alpha - (L_3 + L_4)\sin\theta_4 \end{pmatrix}$$

Expressing Eq. (1.15) in a similar form as Eq. (1.4), the rotation angle θ_4 is resolved as

$$\theta_4 = 2\tan^{-1}\frac{-N_{41} \pm \sqrt{N_{41}^2 + N_{42}^2 - N_{43}^2}}{N_{43} - N_{42}} \tag{1.16}$$

where

$$\begin{cases} N_{41} = -2(y + L_8 \sin\alpha)(L_3 + L_4) \\ N_{42} = -2(x + L_8 \cos\alpha - x_{A2})(L_3 + L_4) \\ N_{43} = (x + L_8 \cos\alpha - x_{A2})^2 + (y + L_8 \sin\alpha)^2 + (L_3 + L_4)^2 - (L_1 + L_2 + L_7)^2 \end{cases}$$

The analytical inverse kineamtic solution are showns in Eqs. (1.9), (1.12), (1.14) and (1.16). Each variable can be generated with one equation, which reveals the decoupled calculation among these four variables.

1.2.2 Forward Kinematics

The forward kinematic model can be constructed through Eqs. (1.1), (1.10), (1.13) and (1.15). In this case, three unknown parameters in $\mathbf{X} = [x; y; \alpha]$ exist in each equation and the calculation process is complicated. Instead of this approach, another straightforward method is utilized in this section according to the special features of this parallel robot. It is not necessary to employ the virtual points G_1 and G_2 within in this alternative approach.

The loop-closure equation in the first kinematic chain is written as

$$\mathbf{OP}_1 = \mathbf{OA}_1 + \mathbf{A}_1\mathbf{C}_1 + \mathbf{C}_1\mathbf{I}_1 + \mathbf{I}_1\mathbf{P}_1 \tag{1.17}$$

Combing Eqs. (1.3) and (1.17) yields the following equations in two orthogonal directions,

$$\Gamma_1 = x_{A1} + (L_1 + L_2 + L_7)\cos\theta_1 + (L_3 + L_4)\cos\theta_2 = x - L_8 \cos\alpha \tag{1.18}$$

$$\Gamma_2 = (L_1 + L_2 + L_7)\sin\theta_1 + (L_3 + L_4)\sin\theta_2 = y - L_8 \sin\alpha \tag{1.19}$$

The vector-loop equation in the second kinematic limb is

$$\mathbf{OP}_2 = \mathbf{OA}_2 + \mathbf{A}_2\mathbf{C}_2 + \mathbf{C}_2\mathbf{I}_2 + \mathbf{I}_2\mathbf{P} \tag{1.20}$$

Equation (1.20) can be resolved into X and Y directions by integrating with the $\boldsymbol{OP}_2$ definition Eq. (1.13),

$$\Gamma_3 = x_{A2} + (L_1 + L_2 + L_7)\cos\theta_3 + (L_3 + L_4)\cos\theta_4 = x + L_8 \cos\alpha \tag{1.21}$$

$$\Gamma_4 = (L_1 + L_2 + L_7)\sin\theta_3 + (L_3 + L_4)\sin\theta_4 = y + L_8 \sin\alpha \tag{1.22}$$

It is noteworthy that the given parameters $\mathbf{Q} = [\theta_1; \theta_2; \theta_3; \theta_4]$ and the desired parameters $\mathbf{X} = [x; y; \alpha]$ are separately in two sides of Eqs. (1.18), (1.19), (1.21) and (1.22). Therefore, the forward kinematic solutions can be directly obtained from these four equations,

$$x = (\Gamma_1 + \Gamma_3)/2 \tag{1.23}$$

$$y = (\Gamma_2 + \Gamma_4)/2 \tag{1.24}$$

$$\alpha = \tan^{-1}[(\Gamma_4 - \Gamma_2)/(\Gamma_3 - \Gamma_1)] \tag{1.25}$$

It is worth noticing that the points $P_1P_2I_2I_1$ and points $P_1P_2H_2H_1$ could not always construct parallelogram linkages within the reachable workspace. A mathematical proof is provided below.

The schematic diagram is illustrated in Fig. 1.2. It is assumed that there is one point G_3 on the line H_1P_1, and one point G_4 on the line H_2P_2. These two extra points are both in the same side of linkage P_1P_2. The lengths of G_3P_1 and G_4P_2 are both equal to ΔL.

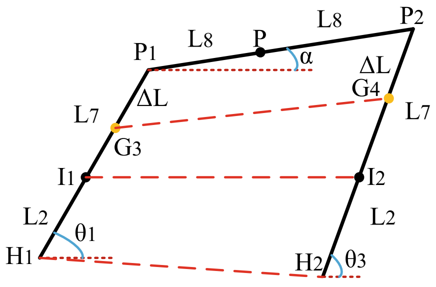

Fig. 1.2 The diagram for linkages $H_1I_1P_1$ and $H_2I_2P_2$

Based on the geometrical relationship, the moving platform P_1P_2 can be solved as

$$\mathbf{P}_1\mathbf{P}_2 = \begin{pmatrix} 2L_8 \cos\alpha \\ 2L_8 \sin\alpha \end{pmatrix} \tag{1.26}$$

The coordinates of two points G_3 and G_4 are calculated separately as

$$\mathbf{OG}_3 = \mathbf{OP}_1 + \mathbf{P}_1\mathbf{G}_3 = \begin{pmatrix} x_{P1} + \Delta L \cos\theta_1 \\ y_{P1} + \Delta L \sin\theta_1 \end{pmatrix} \tag{1.27}$$

$$\mathbf{OG}_4 = \mathbf{OP}_2 + \mathbf{P}_2\mathbf{G}_4 = \begin{pmatrix} x_{P1} + 2L_8 \cos\alpha + \Delta L \cos\theta_3 \\ y_{P1} + 2L_8 \sin\alpha + \Delta L \sin\theta_3 \end{pmatrix} \tag{1.28}$$

where $\mathrm{x_{P1}}$, $\mathrm{y_{P1}}$ are respectively the X and Y components of the point P_1.

The virtual linkage G_3G_4 are then obtained on the basis of Eqs. (1.27) and (1.28)

$$\mathbf{G}_3\mathbf{G}_4 = \mathbf{OG}_4 - \mathbf{OG}_3 = \begin{pmatrix} \Delta L(\cos\theta_3 - \cos\theta_1) + 2L_8 \cos\alpha \\ \Delta L(\sin\theta_3 - \sin\theta_1) + 2L_8 \sin\alpha \end{pmatrix} \tag{1.29}$$

Comparing the Eqs. (1.26) and (1.29), both the dimensions and the orientations of two linkages are not the same except for the cases where $\theta_1 = \theta_3$(The rotation angle beyond 2π rad (e.g., $\theta_1 = \theta_3 + 2k\pi$, k is an integer.) in mathematics can not be reached on this parallel robot). The points $P_1P_2G_4G_3$ can not form a parallelogram linkage. This generic conclusion also testifies that the points $P_1P_2I_2I_1$ and points $P_1P_2H_2H_1$ could not form parallelogram linkages in any robot configuration.

1.2.3 Velocity Relationship

The velocity relationship between actuation velocity $\dot{\mathbf{Q}}$ and mobile platform velocity $\dot{\mathbf{X}}$ can be revealed by the Jacobian matrix. The velocity relationship can be derived from two groups of equations, Eqs. (1.1), (1.10), (1.13), (1.15), and Eqs. (1.18), (1.19), (1.21), (1.22). According to the special configuration of this 2T1R (T and R represent translation and rotation respectively) parallel robot, the orientation of each moving linkage can be directly generated from either the acuation input $\boldsymbol{Q}$ or the mobile platform pose $\boldsymbol{X}$. As a result, the Jacobian matrix obtained from either category of equations contains no unknown passive joint position or rotary angle. However, the latter group of equations is selected for the computation in this section for the sake of simplicity.

Take the differential for Eqs. (1.18), (1.19), (1.21), (1.22) with respect to time and arrange them into the following form,

$$\mathbf{J}_Q\dot{\mathbf{Q}} = \mathbf{J}_X\dot{\mathbf{X}} \tag{1.30}$$

where

$$\mathbf{J}_Q = diag(-(\mathrm{L1} + \mathrm{L2} + \mathrm{L7})\mathrm{sin}\theta_1, (\mathrm{L3} + \mathrm{L4})\mathrm{cos}\theta_2,$$
$$-(\mathrm{L1} + \mathrm{L2} + \mathrm{L7})\mathrm{sin}\theta_3, (\mathrm{L3} + \mathrm{L4})\mathrm{cos}\theta_4)$$

$$\mathbf{J}_X = \begin{bmatrix} -1 & 0 & -L_8\mathrm{sin}\alpha \\ 0 & -1 & L_8\cos\alpha \\ -1 & 0 & L_8\mathrm{sin}\alpha \\ 0 & -1 & -L_8\cos\alpha \end{bmatrix}$$

The Jacobian matrix of this parallel mechanism is then defined as

$$\mathbf{J} = \mathbf{J}_Q^{-1}\mathbf{J}_X \tag{1.31}$$

1.3 Reachable Workspace Determination

The reachable workspace analysis seeks the set of all the qualified positions and orientations the mobile platform can reach. The spatial searching algorithm [21] based on the inverse kinematic model is employed to determine the reachable workspace in this section. The analytical direct kinematic model is not chosen because extra procedures should be supplied since there are only three independent variables in $\boldsymbol{Q}$ (in another word, one variable in $\boldsymbol{Q}$ are dependent on the remaining three variables). The linkage dimensions are provided: $L_1 = L_2 = L_3 = 100$ mm, $L_4 = 150$ mm, $L_5 = L_6 = 0$, $L_7 = 125$ mm, $L_8 = 80$ mm. The coordinates along X direction of two points A_1 and A_2 are given as $\mathrm{x}_{\mathrm{A1}} = 0$, $\mathrm{x}_{\mathrm{A2}} = 500$ mm.

The strokes of the active and passive rotary joints are practically mentioned in the ranges of motion of four actuation rotary joints, as provided below

$$\begin{cases} 0 + \sigma < \theta_1 < \pi - \sigma \\ 0 + \sigma < \theta_2 < \pi/2 - \sigma \\ 0 + \sigma < \theta_3 < \pi - \sigma \\ \pi/2 + \sigma < \theta_4 < \pi - \sigma \end{cases} \tag{1.32}$$

where σ is a manually defined actuation joint angular distance to the unexpected configurations (especially the singularities and their surounding regions)

Equation (1.32) with the absence of σ is the theoretical motion constriants of four driving joints. This parameter could gurantee the avoidance of undesired regions of the mobile platform. σ is equal to $\pi/36$ in this scenario.

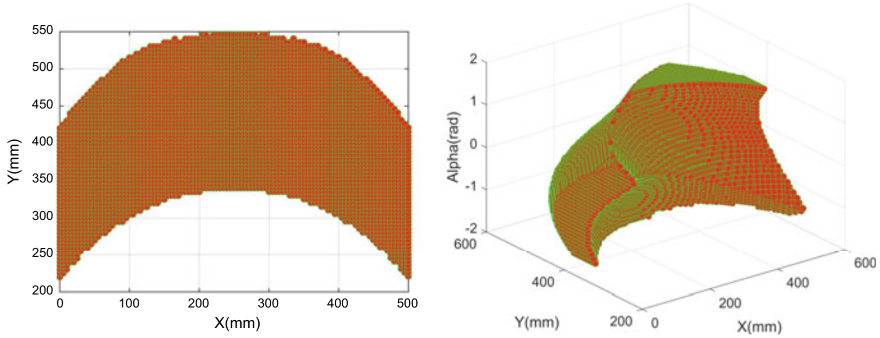

(a) Positions of the mobile platform

(b) Poses of the mobile platform

Fig. 1.3 The reachable workspace

On the basis of the robot configuration demonstrated in Fig. 1.1a, additional limitations are provided to enable the proper operation of the whole structure within the workspace.

$$\begin{cases} \theta_1 > \theta_2 \\ \theta_4 > \theta_3 \end{cases} \tag{1.33}$$

The research workspace of this symmetric parallel mechanism is illustrated in Fig. 1.3. The position distribution of the mobile platform is a symmetrical shape about line X = 250 mm. When the workspace is far away from the symmetrical line, both the upper and lower limits present downward trends. The Y-direction range in each fixed X coordinate is about 210 mm. From Fig. 1.3b, the orientational capacity of the mobile platform in each position varies. The mobile platform can achieve the largest rotational range [-1.4835, 1.4835] rad when point P is close to (250, 450) mm.

1.4 Kinematic Performance Evaluations

The kinematic performance measurements are fundamental to evaluate a parallel robot. The local condition index and manipulability measure are the most widely employed performance indices among all performance indices based on the geometric Jacobian matrix. The latter index is selected in this research. The manipulability measure (MM) proposed by Tsuneo Yoshikawa [22, 23] can evaluate the manipulation capacity of the first-order kinematics for a serial or parallel robot. This index is derived as

$$\text{Manipulability measure} = 1/\sqrt{\det(\mathbf{J}^{\mathrm{T}}\mathbf{J})} \tag{1.34}$$

The layouts of the manipulability measure under three conditions are illustrated in Fig. 1.4. The orientation angle is set as 0 in Fig. 1.4a. The manipulability measure plot is symmetric about line X = 250 mm. This index has a downward trend when the X coordinate is far away from the symmetric line. The Y position of point P is equal to 450 mm in Fig. 1.4b. Its distribution is similar to a saddle surface. Given a constant orientational angle, the manipulability measure increases when the X coordinate is away from both the left and right borders. The X position component of point P is predefined as 250 mm in Fig. 1.4c. This layout has a symmetrical line $\alpha = 0$. The manipulability measures with a constant Y value are close, while the index increases significantly when the Y value decreases and the orientation angle is a constant value.

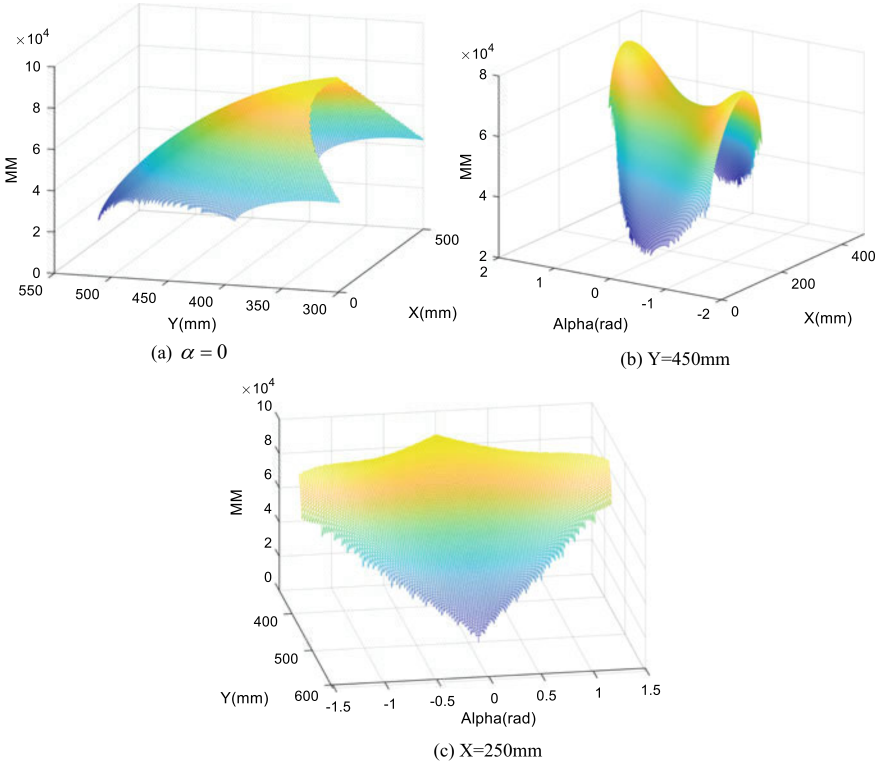

(a) $\alpha = 0$

(b) Y=450mm

(c) X=250mm

Fig. 1.4 The distribution of the Manipulability measure (MM)

1.5 Conclusions

The research presents a novel symmetrical planar parallel architecture based on four parallelogram linkages. This actuation redundant robot could achieve 2 translations and 1 rotation with 4 actuators mounted on the ground. Based on the parallelogram linkages employed in each kinematic limb, all these driven rotary joints (excluding two joints connected to the mobile platform) can be simply calculated from the driving joint variables. This feature significantly simplifies the calculation process of both the inverse and direct kinematic solutions, and provides convenience to derive the Jacobian matrix from both models. The mathematical proof is provided to testify that two linkages H_1P_1 and H_2P_2 are not always paralell to each other even the usage of four parallelogram linkages in the whole structure. This robot has the potential to be utilized as the planar sorting robot, spraying robot and etc. The future work includes investigating singularity avoidance and experimental testification.

Acknowledgements This research was supported by the University Grants from Columbus State University, Basic Science Research Program through the National Research Foundation of Korea (NRF) funded by Ministry of Education (2021R1I1A4A01051258) and in part by the research fund of Hanyang University (HY-2023-0340).

References

1. Zhou, Z., Gosselin, C.M.: Analysis and design of a novel compact three-degree-of-freedom parallel robot. J. Mech. Robot. **15**(5), 051009 (2023)
2. Ye, W., Chai, X.X., Zhang, K.T.: Kinematic modeling and optimization of a new reconfigurable parallel mechanism. Mech. Mach. Theory **149**, 103850 (2020)
3. Luo, X., Xie, F.G., Liu, X.J., Xie, Z.H.: Kinematic calibration of a 5-axis parallel machining robot based on dimensionless error mapping matrix. Robot. Comput. Integr. Manuf. **70**, 102115 (2021)
4. Belzile, B., Eskandary, P.K., Angeles, J.: Workspace determination and feedback control of a pick-and-place parallel robot: analysis and experiments. IEEE Robotics Autom. Lett. **5**(1), 40–47 (2019)
5. Zhou, M.C., Yu, Q.M., Huang, K., Mahov, S., Eslami, A., Maier, M., Lohmann, C.P., Navab, N., Zapp, D., Knoll, A., Nasseri, M.A.: Towards robotic-assisted subretinal injection: a hybrid parallel–serial robot system design and preliminary evaluation. IEEE Trans. Ind. Electron. **67**(8), 6617–6628 (2019)
6. Kim, J., Park, F.C.: Direct kinematic analysis of 3-RS parallel mechanisms. Mech. Mach. Theory **36**(10), 1121–1134 (2001)
7. Yang, C.F., Zheng, S.T., Jin, J., Zhu, S.B., Han, J.W.: Forward kinematics analysis of parallel manipulator using modified global Newton-Raphson method. J. Cent. South Univ. Technol. **17**(6), 1264–1270 (2010)
8. Schreiber, L.T., Gosselin, C.M.: Physical human-robot interaction with a backdrivable (6+3)-dof parallel mechanism
9. Zhang, D., Lei, J.H.: Kinematic analysis of a novel 3-DOF actuation redundant parallel manipulator using artificial intelligence approach. Robot. Comput. Integr. Manuf. **27**(1), 157–163 (2011)

10. Yang, X., Zhu, L.M., Ni, Y.B., Liu, H.T., Zhu, W.L., Shi, H., Huang, T.: Modified robust dynamic control for a diamond parallel robot. IEEE/ASME Trans. Mechatron. **24**(3), 959–968 (2019)
11. Clavel, R.: Device for the movement and positioning of an element in space, US Patent No. 4,976,582 (1990)
12. Bouri, M., Clavel, R.: The linear delta: Developments and applications. In: ISR 2010 (41st International Symposium on Robotics) and ROBOTIK 2010 (6th German Conference on Robotics), pp. 1–8. VDE (2010)
13. Liu, Y., Kong, M., Wan, N., Ben-Tzvi, P.: A geometric approach to obtain the closed-form forward kinematics of h4 parallel robot. J. Mech. Robot. **10**(5), 051013 (2018)
14. Tsai, L.W.: Robot Analysis: The Mechanics of Serial and Parallel Manipulators. Wiley, New York (1999)
15. Kang, L., Oh, S.M., Kim, W.K., Yi, B.Y.: Design of a new gravity balanced parallel mechanism with Schönflies motion. Proc. Inst. Mech. Eng. Part C J. Mech. Eng. Sci. **230**(17), 3111–3134 (2016):
16. Pierrot, F., Nabat, V., Company, O., Krut, S., Poignet, P.: Optimal design of a 4-DOF parallel manipulator: from academia to industry. IEEE Trans. Robot. **25**(2), 213–224 (2009)
17. Chablat, D., Rolland, L.: Design of mechanisms with scissor linear joints for swept volume reduction. In The 4th Joint International Conference on Multibody System Dynamics (2016)
18. Yang, Y., Peng, Y., Pu, H.Y., Chen, H.J., Ding, X.L., Chirikjian, G.S., Lyu, S.N.: Deployable parallel lower-mobility manipulators with scissor-like elements. Mech. Mach. Theory **135**, 226–250 (2019)
19. Gosselin, C.M., Schreiber, L.T.: Redundancy in parallel mechanisms: a review. Appl. Mech. Rev. **70**(1), 010802 (2018)
20. Luces, M., Mills, J.K., Benhabib, B.: A review of redundant parallel kinematic mechanisms. J. Intell. Robot. Syst. **86**, 175–198 (2017)
21. Gosselin, C.M., Schreiber, L.T.: Kinematically redundant spatial parallel mechanisms for singularity avoidance and large orientational workspace. IEEE Trans. Robot. **32**(2), 286–300 (2016)
22. Yoshikawa, T.: Manipulability of robotic mechanisms. Int. J. Robot. Res. **4**(2), 3–9 (1985)
23. Cardou, P., Bouchard, S., Gosselin, C.M.: Kinematic-sensitivity indices for dimensionally nonhomogeneous Jacobian matrices. IEEE Trans. Robot. **26**(1), 166–173 (2010)

Chapter 2
Accelerating Robotics Test and Evaluation with a Streamlined Simulation Process

Vikram Adipudi, Kevin Carey, Andre Harrison, Jeffrey W. Herrmann, Craig Lawrence, James Michaelis, and Adam Porter

Abstract Simulation is a popular approach for testing and evaluating robotic systems, but it is also a challenge due to the complexity of the autonomy stack (the software that runs the robot) and its interactions with the simulation software. This paper describes software tools that streamline the process of creating and running simulation models with unmanned ground vehicles that are using the ARL ground autonomy stack. Using these tools simplifies the tasks that are needed to conduct a simulation study by employing a map-based user interface, providing a checklist for selecting the topics that should be recorded, and automatically iterating over different combinations of configurations and maps. The streamlined process can accelerate the development of safe, reliable robotic systems.

The research described in this paper was supported by Army Cooperative Agreement W911NF2120076.

V. Adipudi · K. Carey · J. W. Herrmann (✉)
Institute for Systems Research, University of Maryland, College Park, MD, USA
e-mail: jwh2@umd.edu

V. Adipudi
e-mail: vadipudi@umd.edu

K. Carey
e-mail: kcarey13@umd.edu

A. Harrison · J. Michaelis
DEVCOM Army Research Laboratory, Adelphi, MD, USA
e-mail: andre.v.harrison2.civ@army.mil

J. Michaelis
e-mail: james.r.michaelis2.civ@army.mil

C. Lawrence
ARLIS, University of Maryland, College Park, MD, USA
e-mail: clawren4@umd.edu

A. Porter
Department of Computer Science, University of Maryland, College Park, MD, USA
e-mail: aporter@umd.edu

P. Larochelle et al. (eds.), *Proceedings of MSR-RoManSy 2024*, Mechanisms and Machine Science 159, https://doi.org/10.1007/978-3-031-60618-2_2